PAH distribution indices, factor analysis, Bonny river. *ARPN J. Earth Sci.*, 2012, **1**, 9–20.
13. Brassell, S. C., Eglington, G., Maxwell, J. R. and Philp, R. P., Natural background of alkanes in the aquatic environment. In *Aquatic Pollutants: Transformation and Biological Effects*, Pergamon Press, Oxford, 1978, pp. 69–86.
14. Punyu, V. R., Harji, R. R., Bhosle, N. B. and Sawant, S. S., *n*-Alkanes in surficial sediments of Visakhapatnam Harbour, east coast of India. *J. Earth Syst. Sci.*, 2013, **122**, 467–477.
15. Farrington, J. W. and Tripp, B. W., Hydrocarbons in western North Atlantic surface sediments. *Geochim. Cosmochim. Acta*, 1997, **41**, 1627–1641.
16. Ekpo, B. O., Oyo-Ita, O. and Wehner, H., Even *n*-alkane/alkene predominances in surface sediments from the Calabar River, S.E. Niger Delta, Nigeria. *Naturwissenschaften*, 2005, **92**, 341–346.
17. Elias, V. O., Simoneit, B. R. T. and Cardoso, J. N., Even *n*-alkane predominances on the Amazon Shelf and a Northeast Pacific Hydrothermal System. *Naturwissenchaften*, 1997, **84**, 415–420.
18. Hu, L., Guo, Z., Feng, J., Yang, Z. and Fang, M., Distributions and sources of bulk OM and aliphatic hydrocarbons in the surface sediments of the Bohai Sea, China. *Mar. Chem*., 2009, **113**, 197–211.
19. Mille, G., Asia, L., Guiliano, M., Malleret, L. and Doumenq, P., Hydrocarbons in coastal sediments from the Mediterranean Sea (Gulf of Fos area, France). *Mar. Pollut. Bull.*, 2007, **54**, 566–575.
20. Grimalt, J. and Albaiges, J., Sources and occurrence of C12–C22 *n*-alkane distributions with even carbon number preference in sedimentary environments. *Geochim. Cosmochim. Acta*, 1987, **51**, 1379–1384.
21. Ahad, J. M. E., Ganeshram, R. S., Bryant, C. L., Cisneros-Dozale, L. M., Ascough, P. L., Fallick, A. E. and Slater, G. L., Sources of *n*-alkanes in an urbanized estuary: insights from molecular distributions and compound-specific stable and radiocarbon isotopes. *Mar. Chem.*, 2011, **126**, 1–4.
22. Pearson, A. and Eglinton, T. I., The origin of *n*-alkanes in Santa Monica Basin surface sediment: a model based on compound-specific $\delta^{14}C$ and $\delta^{13}C$ data. *Org. Geochem.*, 2000, **31**, 1103–1116.
23. Ishiwatari, R., Hirakawa, Y., Uzaki, M., Yamada, K. and Yada, T., Organic geochemistry of the Japan Sea sediments: 1. Bulk organic matter and hydrocarbon analyses of core KH-79-3, C-3 from the Oki Ridge for paleoenvironment assessment. *J. Oceanogr*., 1994, **50**, 179–195.
24. Jeng, W., Higher plant *n*-alkanes average length as an indicator of petrogenic hydrocarbon contained in marine sediments. *Mar. Chem*., 2006, **102**, 242–251.
25. Rao, K. L., *India's Water Wealth, its Assessment, Uses and Projections*, Orient Longman, New Delhi, 1975, p. 255.
26. Balakrishna, K. and Probst, J. L., Organic carbon transport and C/N ratio variations in a large tropical river: Godavari as a case study, India. *Biogeochemistry*, 2005, **73**, 457–473.
27. Tripathy, G. R., Singh, S. K., Bhushan, R. and Ramaswamy, V., 2010. Sr–Nd isotope composition of the Bay of Bengal sediments: impact of climate on erosion in the Himalaya. *Geochem. J.*, 2011, **45**, 175–186.

ACKNOWLEDGEMENTS. We thank the Director, National Institute of Ocean Technology (Ministry of Earth Sciences, Government of India), Chennai for the vessel (*CRV Sagar Purvi*) and the Captain and crew for cooperation on-board. We also thank the Director, Central Water Commission, Hyderabad for the discharge data, and the Council of Scientific and Industrial Research, New Delhi (CSIR No. 21(0802)/10/EMR-II) for financial assistance.

Received 18 January 2014; revised accepted 3 November 2014

Polarimetric classification of C-band SAR data for forest density characterization

A. O. Varghese* and A. K. Joshi

Regional Remote Sensing Centre-Central,
National Remote Sensing Centre, Nagpur 440 001, India

Polarimetric classification is one of the most significant applications of synthetic aperture radar (SAR) remote sensing. Sensitivity of C-band SAR in discerning the variation in canopy roughness and limited penetration capability through forest canopy have been well studied at a given frequency, polarization and incidence angle. However, the scope of C-band SAR in characterizing and monitoring forest density has not been adequately understood with polarimetric techniques. The objectives of the present study were to understand the scattering behaviour of different land-cover classes and evaluate the feasibility of polarimetric SAR data classification methods in forest canopy density slicing using C-band SAR data. The RADARSAT-2 image with fine quad-pol obtained on 27 October 2011 over Madhav National Park, Madhya Pradesh, India and its surroundings was used for the analysis. Forest patches exhibit α-angle around 45°, which means the dominant scattering mechanism is volume; entropy of one or a value close to it denotes distributed targets and low anisotropy values than all other land units, which shows a dominant first scattering mechanism. This study comparatively analysed Wishart supervized classifier and Support Vector Machine (SVM) classifier for classification of the forest canopy density along with other associated land-cover classes for a better understanding of the class separability. All forest density classes showed comparatively good separability in Wishart supervized classification (73.8–84.7%) and in SVM classifier (82.3–84.8%). The results demonstrate the effectiveness of SVM classifier (88.7%) over Wishart supervized classifier (87.8%) with kappa coefficient of 0.86 and 0.85 respectively. The experimental results obtained with polarimetric C-band SAR data over dry deciduous forest area imply that SAR data have a significant potential for estimating stand density in operational forestry.

Keywords: Forest density, microwave radiation, polarimetric classification, synthetic aperture radar.

FOREST cover mapping based on species identification and forest density is an important activity for forest management and biomass estimation, which in turn is crucial for global environmental monitoring. India is among the few countries in the world to start such a unique system of monitoring of forest cover at the national level. At present, Indian forests are monitored by optical remote

*For correspondence. (e-mail: vargheseao@rediffmail.com)

sensing data based on canopy crown density[1]. Most of the data in the assessment pertain to October–December season and non-availability of cloud-free data is a major impediment for the estimation. The ability of C-band microwave energy to penetrate within forest vegetation makes it possible to extract information on crown components, which in turn gives a better approximation of stand density than optical data-derived canopy crown density. Synthetic aperture radar (SAR) signal, being sensitive to plant canopy structure, size, orientation and moisture content of leaves, branches and trunks, is useful for forest density mapping. The literature provides details regarding the use of radar data for many types of application and microwave radar have often shown to be more capable of certain remote sensing tasks than optical or thermal data[2]. Microwave interactions are sensitive to the roughness and physical geometry of forests[3,4]. This, when combined with the ability of microwave radiation to penetrate forest canopies results in a sensitivity of SAR backscatter to key biophysical variables such as tree density and aboveground biomass[5–10]. In a comparative evaluation of multi-frequency, multi-polarized SAR response to plant density, highest sensitivity to plant density was observed in L-band cross-polarized backscatter[11]. The cross-polarization ratio (HV/HH and HV/VV) has been found to be the best parameter for retrieval of forest vegetation parameters[5,6,10,12,13]. Many of the studies related to application of SAR in forestry are reported from temperate regions and few studies were attempted in tropical regions. In Indian tropical regions, various attempts have been made to establish the relationship between radar backscatter in C-, L- and P-bands and forest stand variables[14,15]. Alappat *et al.*[16] have reported good correlation between L-band HV backscatter and forest stand volume, whereas L-band HH backscatter showed good correlation with forest stand density. The objective of the present study was to evaluate the feasibility of polarimetic SAR data classification methods in forest canopy density classification using C-band data.

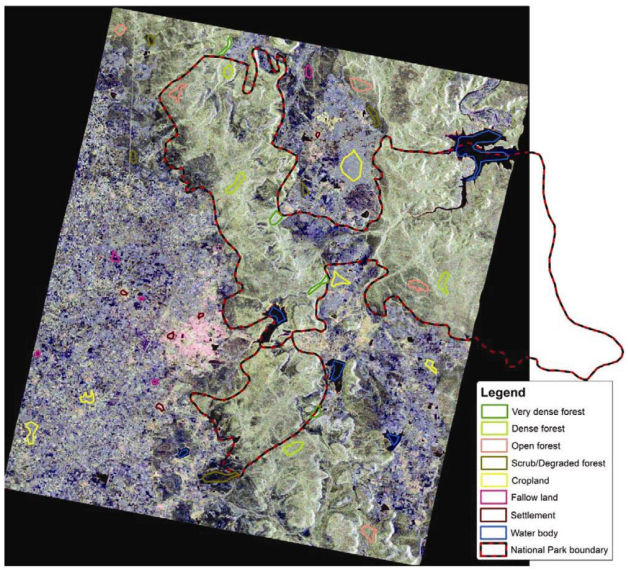

Figure 1. The extent of the study area shown on PauliRGB image.

Madhav National Park, one of the oldest National Parks (354 sq. km) in Madhya Pradesh, India, established in 1956, was taken as the study site along with its surrounding areas (Figure 1). The Park is bounded by geo-coordinates 77°15′–78°30′E and 24°50′–25°55′N. The forests of this Park are tropical dry deciduous and exhibit considerable variation in species gregariousness and densities. Major vegetation types following the forest type classification of Champion and Seth[17] are gregarious formations of *Anogeissus pendula*, *Boswellia serrata*, *Butea monosperma*, *Acacia catechu* and dry deciduous forest. The RADARSAT-2 image with the fine quad-pol (FQ5) and single look complex (SLC) obtained on 27 October 2011 was used in this study. The image has a full polarization of HH, HV, VH and VV, with a range resolution of 4.73 m and azimuth resolution of 4.96 m (1 : 1.05).

Polarimetric target decomposition is a technique that helps in understanding the scattering mechanism involved when a target interacts with SAR. The Radarsat 2 data of the study area were imported in PolSARpro software to generate scattering matrix and thus by coherency matrix. The reflectivity of the area being observed at a given radar wavelength can be represented by a 'scattering matrix' as shown below

$$[S] = \begin{bmatrix} S_{HH} & S_{HV} \\ S_{VH} & S_{VV} \end{bmatrix}.$$

Each of the four complex elements of this matrix is the amplitude and phase of the backscattered radiation as measured at one of four orthogonal transmit/receive polarizations – HH, HV, VH and VV. In radar polarimetry, scattering matrix is transformed into vector format in order to achieve decompositions. Thus, the target vector k_p can be constructed based on the Pauli basis

$$k_p = \frac{1}{\sqrt{2}} \begin{bmatrix} S_{HH} + S_{VV} \\ S_{HH} - S_{VV} \\ 2S_{HV} \end{bmatrix}.$$

With the vectorization a coherency matrix $[T]$ can be generated as

$$[T] = \left\langle \vec{k}_p \cdot \vec{k}_p^{T} \right\rangle,$$

$$[T] = \frac{1}{2} \begin{pmatrix} \langle |S_{HH} + S_{VV}|^2 \rangle & \langle (S_{HH} + S_{VV}) (S_{HH} - S_{VV})^* \rangle & 2\langle (S_{HH} + S_{VV}) \times S_{HV}^* \rangle \\ \langle (S_{HH} - S_{VV}) (S_{HH} + S_{VV})^* \rangle & \langle |S_{HH} - S_{VV}|^2 \rangle & 2\langle (S_{HH} - S_{VV}) \times S_{HV}^* \rangle \\ 2\langle S_{HV} \times (S_{HH} + S_{VV})^* \rangle & 2\langle S_{HV} \times (S_{HH} - S_{VV})^* \rangle & 4\langle |S_{HV}|^2 \rangle \end{pmatrix}$$

This is a 3 × 3 positive semi-definite hermitian coherency matrix where the superscript T denotes the matrix transpose. The $\sqrt{2}$ on the term is to ensure consistency in the span (total power) computation. Speckle confers to SAR images a granular aspect with random spatial variations. Lee sigma filter was used for polarimetric speckle filtering of the data[18,19]. The characteristic decomposition of target coherency matrix for incoherent target decomposition introduced by Cloude[20] was used for the present study. The classification technique used here is based upon polarimetric decomposition classification parameters: entropy (H), anisotropy (A) and alpha (α) angle[21]. The $H/A/\alpha$ set of parameters was derived from an eigenvalue decomposition of the coherency matrix. The eigenvectors and eigenvalues of the coherency matrix $[T]$ were calculated to generate a diagonal form of the coherency matrix which can be physically interpreted as statistical independence between a set of target vectors. Therefore, the eigenvalues of $[T]$ have direct physical significance in terms of the components of scattered power into a set of orthogonal unitary scattering mechanisms given by the eigenvectors of $[T]$, which for radar backscatter forms the columns of a 3 × 3 unitary matrix. Hence an arbitrary coherency matrix can be written in the form

$$[T] = [U_3][\Sigma][U_3]^{-1} = \sum_{i=1}^{i=3} \lambda_i u_i u_i^{*T},$$

where $[\Sigma]$ is a 3 × 3 diagonal matrix with non-negative real elements

$$[\Sigma] = \begin{bmatrix} \lambda_1 & 0 & 0 \\ 0 & \lambda_2 & 0 \\ 0 & 0 & \lambda_3 \end{bmatrix},$$

and $[U_3] = [u_1\ u_2\ u_3]$ is a unitary matrix given by

$$[U_3] = \begin{bmatrix} \cos\alpha_1 & \cos\alpha_2 & \cos\alpha_3 \\ \sin\alpha_1 \cos\beta_1 e^{i\delta_1} & \sin\alpha_2 \cos\beta_2 e^{i\delta_2} & \sin\alpha_3 \cos\beta_3 e^{i\delta_3} \\ \sin\alpha_1 \sin\beta_1 e^{i\gamma_1} & \sin\alpha_2 \sin\beta_2 e^{i\gamma_2} & \sin\alpha_3 \sin\beta_3 e^{i\gamma_3} \end{bmatrix},$$

where u_1, u_2 and u_3 are the three unit orthogonal eigenvectors.

There are three variables of interest to derive, two from the eigenvalues, namely the entropy H and anisotropy A, and one from the eigenvectors, the α angles. The parameter α is an indicator of the type of scattering mechanism, and it ranges from 0° to 90°. These parameters are easily evaluated as[22]

$$\alpha = \sum_{i=1}^{i=3} P_i \alpha_i,$$

P_i are the probabilities obtained from the eigenvalues λ_i

$$0 \le P_i = \frac{\lambda_i}{\sum_{i=1}^{i=3} \lambda_i} \le 1.$$

To introduce the degree of statistical disorder of each target, entropy is defined from the logarithmic sum of eigenvalues of the coherency matrix as

$$H = -\sum_{i=1}^{i=3} P_i \log_3(P_i).$$

The entropy H represents the randomness of the scattering. $H = 0$ indicates a single scattering mechanism (isotropic scattering), while $H = 1$ indicates a random mixture of scattering mechanisms with equal probability and hence a depolarizing target. The anisotropy A is a parameter complementary to the entropy. The anisotropy measures the relative scattering of the second and third eigenvalues of the eigen-decomposition. It is given by

$$A = \frac{\lambda_2 - \lambda_3}{\lambda_2 + \lambda_3}.$$

In the present study, supervized classification techniques like Wishart supervized classifier[23,24] and support vector machine (SVM) classifier[25] have been used for the classification of data. Forest density has been categorized into very dense forest (>70%), dense forest (40–70%), open forest (10–40%) and scrubs and blanks (<10%) according to the classification approach adopted by the Forest Survey of India[1]. The Wishart supervized polarimetric classification scheme performs a maximum likelihood (ML) statistical classification of a polarimetric dataset based on the multivariate complex Wishart probability density function of second-order matrix representations. In the first step, the classifier 'learns' the Wishart statistics of user-defined training areas. The whole dataset is then classified by assigning each pixel to the closest class using a ML decision rule. The SVM theory is based on statistical learning theory and the minimization principle to structure risk. The basic principle of the SVM is to find the optimal linear hyper plane such that the expected classification error for unseen test samples is minimized. On the basis of this principle, a linear SVM uses a systematic approach to find a linear function with the lowest 'Vapnik–Chervonenkis' dimension[25]. For nonlinear separable data, the SVM can map the input to a high dimensional feature space where a linear hyper plane can be found. Therefore, a good generalization can be achieved by the SVM compared to conventional classifiers.

The coherency matrix is closely related to the physical and geometric properties of the scattering process, and thus allows better and direct physical interpretation.

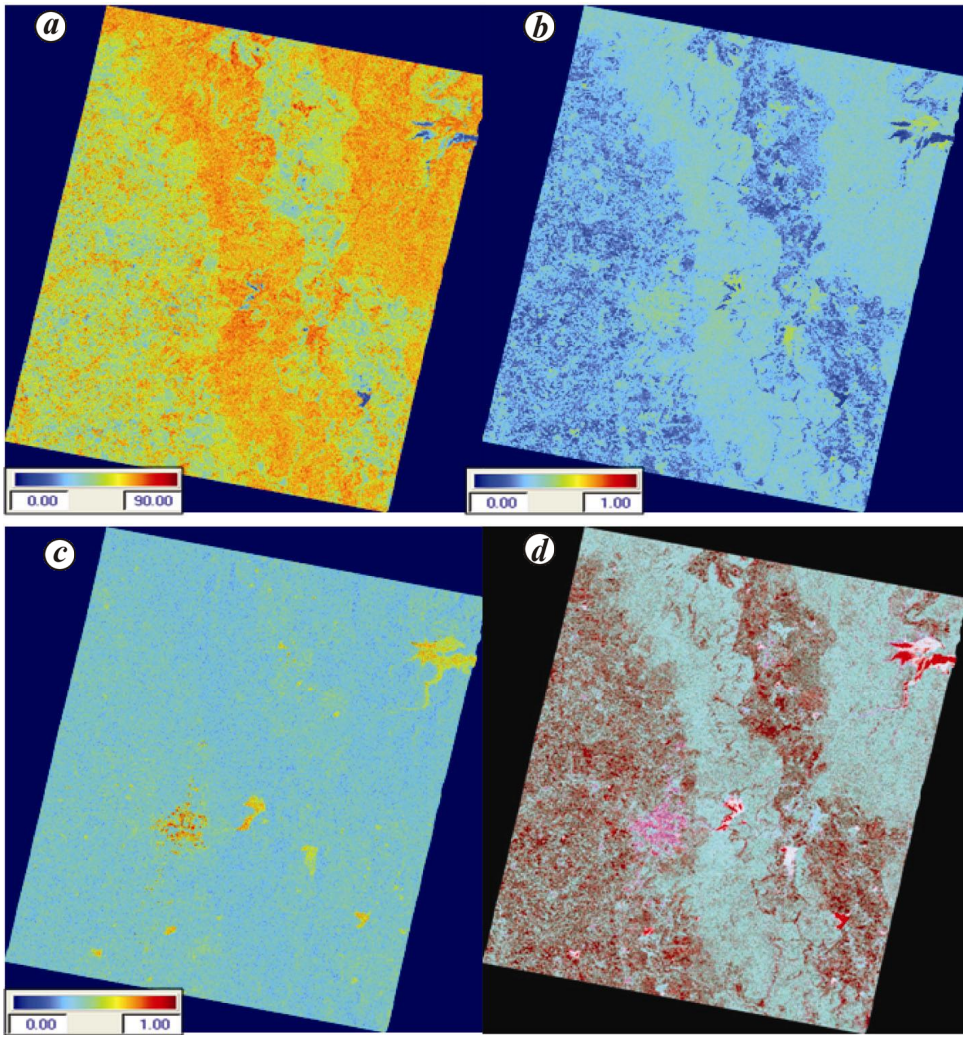

Figure 2. Alpha angle (***a***), entropy (***b***), anisotropy (***c***) and RGB (***d***) of the study area.

Polarimetric target decomposition is a technique that helps in understanding the scattering mechanism that is involved when a target interacts with SAR. The SAR polarimetric analysis leading to the computation of entropy, anisotropy and alpha angle is useful for understanding the scattering process. The first diagonal element of the coherency matrix gives information about single-bounce scattering; the second diagonal element gives information about double-bounce scattering and the third diagonal element gives the information about volume scattering[21].

The model suggested by Cloude and Pottier[21] has been employed to derive entropy, alpha angle and anisotropy segmentation to characterize the image in terms of its scattering mechanism. Alpha angle is indicative of the average or dominant scattering mechanism. It describes the dominance of the scattering mechanism in terms of volume, double bounce or surface scattering. The lower limit of $\alpha = 0°$ indicates surface scattering; $\alpha = 45°$ indicates dipole or volume scattering, while the upper limit of $\alpha = 90°$ represents a dihedral reflector or multiple scattering (Figure 2 *a*). As represented in Figure 2 *a*, much of the study area exhibits α-angle around 45°, which means the dominant scattering mechanism is volume. Dihedral reflector or multiple scattering occurs in the settlement area. Entropy is a measure that indicates the randomness in the target vector. For pure targets the entropy is zero, whereas for distributed target entropy is one. In the study area, mainly forest patches show entropy of one or a value close to it denotes distributed targets and water body exhibits entropy of zero (Figure 2 *b*). The entropy–alpha space was not able to distinguish the number of scattering mechanisms and their relative dominance. By introducing anisotropy, which is a measure of the number of dominant scattering mechanisms involved in the scattering process, it is feasible to achieve better discrimination between the different scattering classes[21]. Anisotropy is useful to differentiate scattering mechanisms which have different eigenvalue distributions but similar entropy values. When the entropy values for two clusters

are the same, a high anisotropy value shows two dominant scattering mechanisms with equal chance of occurrence and a less significant third mechanism, whereas a low anisotropy value shows a dominant first scattering mechanism and two insignificant secondary mechanisms with equal importance. Anisotropy gives the homogeneity of a target with reference to the radar look direction. For homogeneous target, low anisotropy value is observed. In the study site forested area mainly exhibits low anisotropy values than all other land units, which shows a dominant first scattering mechanism, i.e. volume scattering and two insignificant secondary mechanisms with equal importance (Figure 2 *c*). Settlement areas show high anisotropy values because of two dominant scattering mechanisms with equal chance of occurrence and a less significant third mechanism.

Wishart supervized classification was performed according to the defined training areas on coherency matrix. A total of eight classes were identified in the study area, including cropland, fallow land, settlement, water body and four forest density classes. The ground truth information collected from the study area using GPS overlaid on 2.5 m resolution Cartosat1 data of Indian remote sensing satellite for cross-checking and verification. This information has been used as training classes in the classification stage. PauliRGB image was used for giving the training areas. The whole dataset was then classified by assigning each pixel to the closest class using a maximum likelihood decision rule (Figure 3). All forest density class pixels show good classification results (above 73.8%) as represented in the confusion matrix (Table 1). Dense forest shows comparatively less percentage (73.8) of correctly classified pixels among the forest density classes. This is mainly because of the misclassification of pixels of this class into open forest. Among other classes, water body pixels show good classification results (98.9%) followed by croplands (84.6%). The overall classification accuracy observed for Wishart supervized classification is 87.8% and kappa coefficient of 0.85.

The SVM method is based on the determination of the optimal hyperplane of the input data space that maximizes the distance separating the training classes. When such a hyperplane cannot be found, training vectors are projected into a higher-dimensional space (the feature space) in which the search for the optimal hyperplane will be replayed. The projection of the problem in the feature space is significantly simplified by the use of a kernel. In a first step, the classifier 'learns' the SVM by defining the hyperplane based on user-defined training areas, and defines a SVM model. The whole dataset is then classified by assigning each pixel to the closest class using the hyperplane side. SVM uses kernel functions to map nonlinear decision boundaries in the original data space into linear ones in a high-dimensional space. There are many kernel functions in SVM like linear, polynomial, radial basic function (RBF) and sigmoid. RBF kernel, which is one of the most popular and has fewer numerical difficulties[26], was used in this study to classify the pixels. The optimization parameter calculated a cost parameter of 16,384 and gamma parameter of one for the classification. The RBF kernel nonlinearly maps samples into a higher dimensional space unlike the linear kernel and RBF has less hyperparameters than the polynomial kernel. The RBF kernel has less numerical difficulties.

SVM supervized classification was performed (Figure 4) on coherency matrix according to the defined training areas which have been used for Wishart supervized

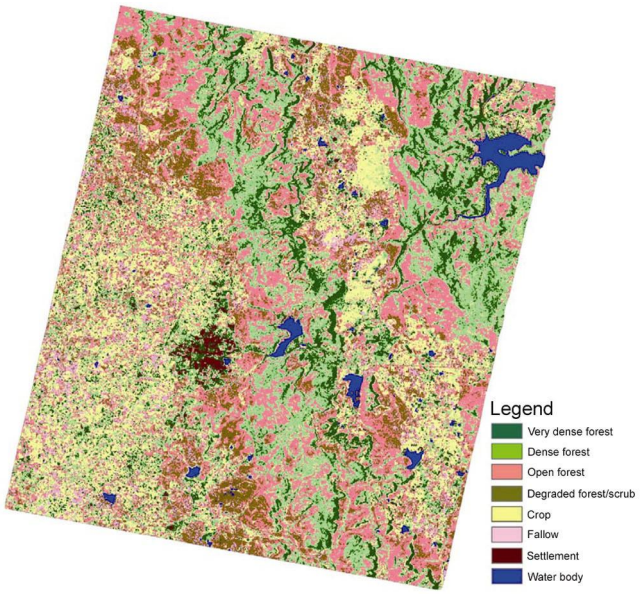

Figure 3. Wishart supervized classification results of the study area.

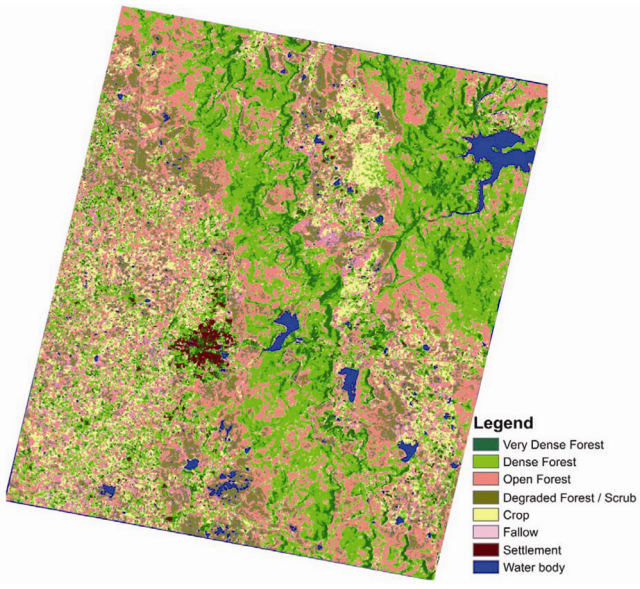

Figure 4. SVM classification results of the study area.

Table 1. Confusion matrix of Wishart supervized classification

	C1	C2	C3	C4	C5	C6	C7	C8
C1 Water body	98.95	0.00	0.00	0.04	0.07	0.06	0.00	0.87
C2 Settlement	0.00	43.49	6.71	0.00	0.38	12.23	37.19	0.00
C3 Cropland	0.00	0.06	84.62	0.20	6.38	8.33	0.37	0.04
C4 Fallow land	0.00	0.00	1.17	58.09	1.09	0.13	0.23	39.30
C5 Open forest	0.00	0.00	3.59	0.01	83.66	11.07	0.00	1.66
C6 Dense forest	0.00	0.02	6.01	0.00	15.64	73.88	4.46	0.00
C7 Very dense forest	0.00	4.01	3.60	0.00	0.59	7.03	84.77	0.00
C8 Degraded forest/scrub	2.85	0.00	0.12	13.79	1.04	0.01	0.00	82.20

Table 2. Confusion matrix of support vector machine classification

	C1	C2	C3	C4	C5	C6	C7	C8
C1 Water body	98.71	0.04	0.00	0.06	0.04	0.04	0.00	1.11
C2 Settlement	0.13	86.93	2.01	0.08	0.20	2.26	8.39	0.00
C3 Cropland	0.00	0.96	89.31	0.71	4.21	4.62	0.19	0.00
C4 Fallow land	0.02	0.26	0.94	66.06	0.32	0.04	0.08	32.28
C5 Open forest	0.00	0.02	2.34	0.35	84.81	11.83	0.00	0.64
C6 Dense forest	0.00	1.50	4.87	0.01	8.44	82.86	2.33	0.00
C7 Very dense forest	0.08	7.53	1.97	0.10	0.42	5.23	84.68	0.00
C8 Degraded forest/scrub	1.65	0.00	0.13	15.10	0.75	0.01	0.00	82.37

classification. All forest density class pixels show better classification accuracy compared to Wishart supervized classification as represented in the confusion matrix (82.3–84.8%). Degraded forest shows comparatively less percentage (82.3) of correctly classified pixels among the forest density classes (Table 2). This is mainly because of the misclassification of pixels of this class into fallow land pixels. Among other classes water body pixels show good classification results (98.7%). The overall accuracy and kappa coefficient observed for SVM supervized classification are 88.74% and 0.86 respectively.

The present study analysed the scattering behaviour of dominant land-cover classes of tropical regions of India and evaluated the feasibility of using polarimetric SAR data classification methods in forest canopy density slicing using C-band SAR data. Forest patches exhibit α-angle around 45°, which means the dominant scattering mechanism is volume; entropy of one or a value close to it denotes distributed targets and low anisotropy values than all other land units, which shows a dominant first scattering mechanism. Wishart supervized classifier and SVM classifier were used for the classification of the SAR data for forest density slicing. All forest density classes show comparatively good separability in Wishart supervized classification (73.8–84.7%) and SVM classifier (82.3–84.8%). Comparative analysis reveals that SVM supervized classifier gives better classification accuracy (88.7% and 0.86) for forest density discrimination than Wishart classifier (87.8% and 0.85) for classification of forest density according to the overall accuracy and kappa coefficient. If classification is considered under forest mask, better accuracy can be achieved. C-band SAR data-derived information on crown components gives a better approximation of stand density than optical data derived canopy crown density. The limitations associated with optical data like non-availability of cloud-free data and misclassification because of gregarious occurrence of bushy vegetation like Lantana can be overcome using C-band SAR data.

1. FSI, India State of Forest Report, 2011. Forest Survey of India, Dehradun, Ministry of Environment & Forests, Government of India, 2011, p. 294.
2. Shakil, A. R. and Masanobu, S., Employing SAR for retrieval from tropical forests of Southeast Asia. In Proceedings of 22nd Asian Conference on Remote Sensing, Singapore, 5–19 November 2001.
3. Ferrazoli, P. and Guerriero, L., Radar sensitivity to tree geometry and woody volume: a model analysis. *IEEE Trans. Geosci. Remote Sensing*, 1995, **33**, 360–371.
4. Imhoff, M., Story, M., Vermillion, C., Khan, F. and Polcyn, F., Forest canopy characterization and vegetation penetration assessment with space-borne radar. *IEEE Trans. Geosci. Remote Sensing*, 1986, **24**, 535–542.
5. Le Toan, T., Beaudoin, A., Riom, J. and Guyon, D., Relating forest biomass to SAR data. *IEEE Trans. Geosci. Remote Sensing*, 1992, **37/1**(50), 2249–2259.
6. Dobson, M. C., Ulaby, F. T., Toan, T., Beaudoin, A. E., Kasischke, S. and Christensenm, N., Dependence of radar backscatter on coniferous forest biomass. *IEEE Trans. Geosci. Remote Sensing*, 1992, **30**, 412–415.
7. Baker, J. R., Mitchell, P. L., Cordey, R. A., Groom, G. B., Settle, J. J. and Stileman, M. R., Relationships between physical characteristics and polarimetric radar backscatter for Corsican pine stands in Thetford forest, UK. *Int. J. Remote Sensing*, 1994, **15**, 2847–2849.
8. Beaudoin, A. *et al.*, Retrieval of forest biomass from SAR data. *Int. J. Remote Sensing*, 1994, **15**, 2777–2796.
9. Ranson, K. J. and Sun, G., Mapping biomass of a Northern forest using multi-frequency SAR data. *IEEE Trans. Geosci. Remote Sensing*, 1994, **32**, 388–396.

10. Rauste, Y., Hame, T., Pulliainen, J., Heiska, K. and Hallikainen, M., Radar-based forest biomass estimation. *Int. J. Remote Sensing*, 1994, **15**, 2797–2808.
11. Parul Patel, Srivastava, H. S., Panigrahy, S. and Parihar, J. S., A comparative evaluation of sensitivity of multi-polarized multi-frequency SAR backscatter to plant density. *Int. J. Remote Sensing*, 2006, **27**(2), 293–305.
12. Wu, S. T. and Sader, S. A., Multi-polarization SAR data for surface feature delineation and forest vegetation characterization. *IEEE Trans. Geosci. Remote Sensing*, 1987, **25**(1), 67–76.
13. Green, R. M., Relationship between polarimetric SAR backscatter and forest canopy and sub-canopy biophysical properties. *Int. J. Remote Sensing*, 1998, **19**(12), 2395–2412.
14. Varghese, A. O., Rao, S. S., Rao, D. S., Prakash Rao and Krishnamurthy, Y. V. N., Forest stand mensuration using polarimetric analysis of SAR data. In Proceedings of Conference on Joint Experiment Project towards Microwave Remote Sensing Data Utilization, Space Applications Centre, Ahmedabad, 5–16 May 2007.
15. Vyjayanthi, M., Rangaswamy, M., Jha, C. S. and Murthy, M. S. R., Estimation of biomass from C, L and P-bands of DLR ESAR data. In Proceedings of Conference on Joint Experiment Project towards Microwave Remote Sensing Data Utilization, Space Applications Centre, Ahmedabad, 15–16 May 2007.
16. Alappat, V. O., Joshi, A. K. and Krishnamurthy, Y. V. N., Tropical dry deciduous forest stand variable estimation using SAR data. *J. Indian Soc. Remote Sensing*, 2011, **39**(4), 583–589.
17. Champion, H. G. and Seth, S. K., *A Revised Survey of the Forests Types of India*, Manager of Publications, Government of India, 1968, p. 404.
18. Lee, J. S., Grunes, M. R. and De Grandi, G., Polarimetric SAR speckle filtering and its implications for classification. *IEEE Trans. Geosci. Remote Sensing*, 1999, **37**(5), 2363–2373.
19. Lee, J. S., Wen, J. H., Ainsworth, T., Chen, K. S. and Chen, A. J., Improved sigma filter for speckle filtering of SAR imagery. *IEEE Trans. Geosci. Remote Sensing*, 2009, **47**, 202–213.
20. Cloude, S. R., Group theory and polarization algebra. *Optik*, 1986, **75**(1), 26–36.
21. Cloude, S. R. and Pottier, E., A review of target decomposition theorems in radar polarimetry. *IEEE Trans. Geosci. Remote Sensing*, 1996, **34**, 498–518.
22. Cloude, S. R. and Pottier, E., An entropy based classification scheme for land applications of polarimetric SAR. *IEEE Trans. Geosci. Remote Sensing*, 1997, **35**, 68–78.
23. Lee, J. S., Hoppel, K. W., Mango, S. A. and Miller, A., Intensity and phase statistics of multi-look polarimetric and interferometric SAR Imagery. *IEEE Trans. GE*, 1994, **32**, 1017–1028.
24. Lee, J. S., Grunes, M. R. and Kwok, R., Classification of multi-look polarimetric SAR imagery based on the complex Wishart distribution. *Int. J. Remote Sensing*, 1994, **15**(11), 2299–2311.
25. Vapnik, V., *The Nature of Statistical Learning Theory*, Springer-Verlag, New York, 1995, p. 314.
26. Hsu, C.-W., Chang, C.-C. and Lin, C.-J., A *Practical Guide to Support Vector Classification*, Department of Computer Science, National Taiwan University, 2010; http://www.csie.ntu.edu.tw/cjlin

ACKNOWLEDGEMENTS. We thank V. K. Dadhwal (Director, National Remote Sensing Centre) and J. R. Sharma (Chief General Manager, RCs, Hyderabad) for encouragement and valuable suggestions; the Director, Space Application Centre, Ahmedabad for entrusting this study to RRSC, Nagpur and providing the necessary funds; Manab Chakraborthy (Group Director, GTDG/RESIPA & Project Director, RISAT_UP) for guidance and Shiv Mohan (former Project Director, RISAT_UP) for his keen interest and encouragement. We also thank Arun Suryavamsi and Sivaprasad Reddy for help.

Received 8 May 2014; revised accepted 30 September 2014

Phenological events along the elevation gradient and effect of climate change on *Rhododendron arboreum* Sm. in Kumaun Himalaya

Nandan Singh[1,*], Jeet Ram[1], Ashish Tewari[1] and R. P. Yadav[2]

[1]Department of Forestry and Environmental Science, Kumaun University, Nainital 263 002, India
[2]Vivekananda Institute of Hill Agriculture, ICAR, Almora 263 601, India

Phenological events of rhododendron (*Rhododendron arboreum* Sm.) were monitored along elevation gradients in distinct ecological settings. The observations were carried out between 1500 and 2500 m elevation in Central Himalaya. The phenological events, i.e. bud formation, bud bursting, leafing, flowering, fruit formation and seed formation were recorded. Phenological duration and synchrony of all these phenophases were determined within site and along the elevation gradient in each study site. Our observations showed high synchrony throughout the elevation gradient, especially for peak flowering. Temperature, rainfall, age of the observed trees and site characteristics were related to initial and peak flowering dates. The circumference varied from 35.0 ± 2.73 to 140.0 ± 2.88 cm; similarly, height varied from 5.0 ± 1.02 to 16.5 ± 1.41 m. All the phenological events began early at low elevation and were delayed at higher elevation. *R. arboreum* had a sharp flowering peak from January to March. Wet season flowering was rare, and seed formation occurred in summer. The climatic conditions affected the phenological characters of *R. arboreum*.

Keywords: Climate change, elevation gradient, phenology, *Rhododendron arboreum*.

RHODODENDRON arboreum Sm. (local name – Burans, family – Ericaceae) is one of the most important small, evergreen and a major under canopy tree species in the Central Himalayan forests. It is widely distributed from 1000 to 2500 m elevation in Kumaun Himalaya. Common associates of this tree are about 16 trees and 19 shrubs. At low elevation, it mixes with chir pine and broadleaf species, while at high elevation it remains either as under canopy species in *Quercus semecarpifolia* forest or dominates as canopy species in some location near timberline. *R. arboreum* is distributed from subtropical to temperate forests. The subtropical forests are located along an altitudinal gradient and exhibit limited day length variation within the annual cycle. However, temperature, particularly at higher elevation approaches those of temperate latitudes. Phenological observations provide

*For correspondence. (e-mail: nandansinghm@yahoo.com)